Photochemistry and Photobiology, 2000, 71(6): 730–736

Autofluorescence Patterns in Short-Term Cultures of Normal Cervical Tissue

Carrie K. Brookner[1], Michele Follen[2], Iouri Boiko[2], Javier Galvan[1], Sharon Thomsen[3], Anais Malpica[3], Seigo Suzuki[4], Reuben Lotan[4] and Rebecca Richards-Kortum*[1]

[1]Biomedical Engineering Program and Department of Electrical and Computer Engineering, University of Texas at Austin, Austin, TX;
Departments of [2]Gynecologic Oncology, [3]Pathology and [4]Tumor Biology, U. T. M. D. Anderson Cancer Center, Houston, TX.

Received 15 November 1999; accepted 25 February 2000

ABSTRACT

Fluorescence spectroscopy has potential to improve cervical precancer detection. The relationship between tissue biochemistry and fluorescence is poorly understood. The goal of this study was to characterize normal cervical autofluorescence, using fresh tissue short-term tissue cultures and epithelial cell suspensions. Transverse, short-term tissue cultures were prepared from 31 cervical biopsies; autofluorescence images were obtained at 380 and 460 nm excitation. Fluorescence excitation–emission matrices were measured from normal, precancerous and cancerous cervical cell suspensions. Observed fluorescence patterns contrast those reported for frozen–thawed tissue, and were placed into groups with (1) bright epithelial and weak stromal fluorescence; (2) similar epithelial and stromal fluorescence; and (3) weak epithelial and bright stromal fluorescence. The average ages of women in the groups were 30.9, 38.0 and 49.2 years. Epithelial fluorescence intensity was similar in Groups 1 and 2, but weaker in Group 3. Stromal intensity was similar in Groups 2 and 3, but weaker in Group 1. The ratio of epithelial to stromal fluorescence intensity was significantly different for all groups. EEMs of cell suspensions showed peaks consistent with tryptophan, reduced form of nicotinamide adenine dinucleotide (phosphate) and flavin adenine dinucleotide. Short-term tissue cultures represent a novel, biologically appropriate model to understand cervical autofluorescence. Our results suggest a biological basis for the increased fluorescence seen in older, postmenopausal women.

INTRODUCTION

Fluorescence spectroscopy has the potential to improve the efficacy of cervical precancer detection. Diagnostic algorithms have been developed that can classify tissue as normal or diseased based on fluorescence emission spectra measured *in vivo* (1–5). Algorithms based on fluorescence emission spectra obtained at 337, 380 and 460 nm excitation can identify precancers with a sensitivity and specificity exceeding that of colposcopy in expert hands (3). However, these algorithms were developed empirically; the spectral data were systematically processed to reduce interpatient variations, and algorithms were designed to maximally exploit the differences between data from different tissue categories. The underlying biochemical and morphological changes that occur in the disease and cause such spectral differences are poorly understood. Therefore, the relationship between the tissue properties and the resulting spectra has not been fully utilized to optimize the diagnostic capabilities of fluorescence spectroscopy. Furthermore, unexplained interpatient variations in the intensity of spectral data limit the applicability of current diagnostic algorithms.

Several studies have been performed to elucidate the relationship between fluorescence spectra and the underlying tissue biochemistry and morphology (6–8). For example, Ramanujam *et al.* (6) used a model of turbid tissue fluorescence to describe spectral data acquired from the cervix at 337 nm excitation (6). Results showed that the contribution of collagen fluorescence decreases and the contributions of reduced nicotinamide adenine dinucleotide (NADH)† fluorescence and hemoglobin absorption increase as the tissue progresses from normal to dysplastic. These findings are consistent with histopathologic changes associated with cervical dysplasia. The epithelial thickening, which is commonly seen in dysplastic cervical tissues, could explain the decreased contribution of the collagen fibers that are present in the underlying stroma. It is also hypothesized that abnormal tissues have an increased metabolic rate, and therefore an increased concentration of the reduced electron carriers, NADH and flavin adenine dinucleotide ($FADH_2$), and a decreased concentration of the oxidized electron carriers, NAD^+ and FAD. This difference in metabolic rate could

*To whom correspondence should be addressed at: Biomedical Engineering Program, ENS 610, Austin, TX 78712, USA. Fax: 512-471-0616; e-mail: kortum@mail.utexas.edu

†*Abbreviations:* DMEM, Dulbecco modified Eagle medium; EEM, excitation–emission matrix; FAD, flavin adenine dinucleotide; (H & E), hematoxylin and eosin; KCN, potassium cyanide; LEEP, loop electrosurgical excision procedure; NADH, reduced nicotinamide adenine dinucleotide; NAD(P)H, reduced nicotinamide adenine dinucleotide (phosphate); PBS, phosphate-buffered saline.

contribute to the spectral differences observed between normal and abnormal tissues *in vivo.* An increased contribution of hemoglobin is consistent with the increased vascularization seen in severely dysplastic tissues. One limitation of this study is that it assumed the tissue is a homogeneous layer with a constant scattering coefficient. Durkin *et al.* showed that chromophore concentrations are not reliable when predicted with this type of simplified tissue model (9).

A model was developed by Zonios *et al.* to predict the fluorescence spectra of normal and neoplastic colonic tissue at 370 nm excitation (10). Monte Carlo techniques were used to predict the propagation of photons at the excitation and emission wavelengths. The distribution of fluorophores was measured from fluorescence images of 5 μm–thick transverse frozen–thawed sections, and absorption and scattering coefficients were calculated from *in vitro* measurements of diffuse reflectance and transmission. The predicted spectra exhibited the characteristic differences of normal and abnormal tissues measured *in vivo.*

Fluorescence microscopy and spectroscopy have also been used to examine cervical tissue autofluorescence in 4 μm thick frozen–thawed sections from biopsies. When exciting at 337, 380 and 460 nm, Mahadevan found that epithelial fluorescence was seen only in the most superficial layers, with brighter, more widespread fluorescence present in the stroma (8). Lohmann *et al.* reported similar cervical autofluorescence patterns for frozen–thawed tissue sections at 365 nm excitation (7).

A major limitation of the studies described above is that they were performed using frozen–thawed tissue. Because the metabolic indicators NADH and FAD are potentially important fluorophores, it is important to measure fluorescence from tissue which is in as close a metabolic state to the *in vivo* situation as possible. Schomaker *et al.* showed that the fluorescence of NADH decreases exponentially in the 2 h following tissue removal, as NADH present in the tissue is oxidized to NAD^+, which is nonfluorescent (11). While fast freezing a tissue biopsy can preserve the metabolic state, oxygenation occurs as the sectioned tissue thaws prior to microscopic examination. Therefore, measurements made from frozen–thawed sections are not expected to accurately reflect the autofluorescence present *in situ.* Imaging the autofluorescence of metabolically active tissue would be much more informative.

A microtome that can rapidly prepare fresh tissue slices (12–14) was developed by Krumdieck and colleagues. Using this device, it is possible to produce fresh tissue slices of a consistent thickness with minimal tissue trauma. The optimal thickness of a slice suitable for culture lies between the lower limit of 50–100 μm, where a large percentage of the cells are destroyed at the cut surfaces, and the upper limit of 400–500 μm, where the cells in the center undergo necrosis due to oxygen and nutrient deprivation. The functional integrity of liver slices obtained with this microtome has been studied and tissue is viable in culture for up to 20 h with minimal loss of biochemical function (14).

The goals of this study were to (1) use short-term tissue cultures to characterize normal cervical tissue autofluorescence both qualitatively and quantitatively; (2) contrast autofluorescence observed from short-term tissue cultures of cervical tissue with that of frozen–thawed sections from biopsies; (3) determine if the observed autofluorescence patterns can explain the age-related patient to patient variations in clinical spectral data; and (4) explore which fluorophores are responsible for cervical autofluorescence—this was studied by (1) perturbing the metabolic state of the short-term tissue cultures; (2) using several histological stains; and (3) correlating fluorescence images with fluorescence spectra from epithelial cell suspensions.

METHODS

Slice preparation. Cervical biopsies (2 mm × 4 mm × 1 mm) were obtained, with written consent, from women seen in the University of Texas M. D. Anderson Cancer Center Colposcopy Clinic and the Lyndon B. Johnson Hospital Colposcopy Clinic. These women were being treated for cervical dysplasia with the loop electrosurgical excision procedure (LEEP), or were undergoing a colposcopy examination. Acetic acid (3%) was applied to the cervix during colposcopy in all patients prior to biopsy. Biopsies obtained from women undergoing the LEEP procedure were obtained after the administration of the anesthetic (2% lidocaine), but before treatment. In all but one case, the cervix was also anesthetized before biopsies were obtained from colposcopy patients. Biopsies were immediately placed in chilled culture medium (Dulbecco modified Eagle medium [DMEM] without phenol red), and were then embedded in 4% agarose for slicing. The Krumdieck Tissue Slicer (Alabama Research and Development MD1000-A1) was used to obtain 200 μm–thick fresh tissue slices, which were cut perpendicular to the epithelial surface. Fluorescence images were obtained from tissue slices within 1.5–5 h of biopsy. Control experiments showed that fluorescence intensities were stable to within ±10% immediately following up to 5.5 h postpreparation of the slices.

Fluorescence microscopy. A Zeiss Axiophot 410 inverted fluorescence microscope was used to examine the unstained tissue slices under bright-field and fluorescence conditions. Areas with recognizable epithelium and stroma were identified under bright-field, and autofluorescence images were collected from these areas at 380 and 460 nm excitation, using the 100 W mercury lamp of the microscope and a filter cube with filter sets I (BP382 exciter filter, FT395 dichroic mirror, 397 long-pass filter) and II (BP460 exciter filter, FT510 dichroic mirror, GG475 long-pass filter), respectively. To improve the rejection of the excitation light, the filter sets were modified early in the study to I (BP380 exciter filter, FT410 dichroic mirror, 420 long-pass filter) and II (BP455 exciter filter, FT470 dichroic mirror, GG495 filter). In this study, a subset of tissue slices was also imaged at 337 nm excitation. These slices were illuminated from above with a fiber optic probe coupled to a nitrogen laser, and filter set I was used for collection. The microscope was coupled to a liquid-nitrogen cooled charge-coupled device camera (Photometrics Series 200) and image acquisition was computer controlled using the IPLab image processing software. For each fluorescence image, the appropriate dark current image and the temperature of the camera were recorded. The tissue slices remained in culture medium during the imaging, and an image of a field of medium was collected as a control. All fluorescence images at 380 and 460 nm excitation were collected using a 10× objective and a 5 s exposure time. At 337 nm excitation, a 10 or 15 s exposure was used.

Image analysis. The appropriate dark current image was subtracted from each fluorescence image. To enhance visualization of tissue fluorescence, image contrast was stretched and pseudocolor was added. The average intensity *vs* tissue depth was plotted for each background subtracted, unprocessed image. Intensity *vs* depth was averaged over an image area selected perpendicular to the basement membrane. The width of the selected area was chosen to be as wide as possible, while avoiding features in the images such as holes in the section or areas of extreme clumping. No image areas without tissue were included. Finally, the average intensities in the epithelium and stroma and their ratio (epithelium/stroma) were calculated for each image.

Tissue metabolism. To determine if any region of the autofluorescence pattern observed in the slices was attributable to the electron carriers, NADH and FAD, the metabolic state of the slices was

perturbed with potassium cyanide (KCN). KCN blocks the cytochrome oxidase step of oxidative phosphorylation, and its addition to the medium should shut down this portion of the cellular metabolic pathway. The expected result would be an increase in the concentration of NADH (and $FADH_2$), and therefore a decrease in the concentration of FAD. Measurable changes in the fluorescence due to NADH and FAD in response to KCN have been previously reported (15). After imaging a tissue slice at 380 nm excitation in culture medium, KCN was added to the medium to a final concentration of 5 m*M*. The same area of the slice was then reimaged several times over a 1 h period of exposure to KCN. This experiment was performed with two different slices from two different patients.

Histological staining. Following fluorescence microscopy, tissue slices were fixed in 10% formalin, embedded in paraffin and 4 μm sections were made for histological evaluation. A standard hematoxylin and eosin (H & E) protocol was used to stain sections from each tissue slice; a subset of sections was stained using the Masson's trichrome protocol and the Modified Verhoff's Van Geison (elastin) protocol (16) to determine the presence and distribution of collagen and elastin. Stained sections were used to correlate fluorescent areas to histological features of the tissue. H & E slides were read by a board-certified pathologist with expertise in gynecologic pathology to provide a diagnosis of the particular tissue imaged.

Excitation–emission matrices of cell suspensions. Fluorescence excitation–emission matrices (EEMs) were measured from suspensions of two cervical cancer cell lines (HeLa and SiHa), HPV-18 immortalized cervical epithelial cells (TCL-1) and normal ectocervical cells from primary culture (CrEC-Ec). HeLa and SiHa cells were obtained from the American Type Culture Collection (Rockville, MD); TCL-1 cells were obtained from Dr. Vitorio Defendi (New York University, New York, NY); CrEC-Ec cells were obtained from Clonetics (Walkersville, MD). The HeLa cells harbor HPV-18 and the SiHa cells HPV-16. The neoplastic and preneoplastic cell lines were cultured in DMEM growth medium and Ham's F12 (GIBCO, Grand Island, NY) supplemented with 5% (vol/vol) fetal bovine serum (GIBCO) and antibiotics (100 Units/mL penicillin and 100 mg/mL streptomycin). TCL-1 cells were grown in DMEM:F12 supplemented with 10% Nuserum (Becton Dickinson Co., Franklin Lakes, NJ), 10 m*M* *N*-2-hydroxyethylpiperazine-*N*′-2-ethane-sulfonic acid buffer (Sigma Chemical Co., St. Louis, MO), 0.5 μg/mL hydrocortisone (Sigma) and 10 ng/mL human epidermal growth factor (Promega, Madison, WI). The normal cells were cultured through 1 passage in keratinocyte growth medium-2 (Clonetics). The cell cultures were routinely checked for mycoplasma and were found to be free of contamination. The cultures were dispersed by repeated pipeting after brief incubation with 2 m*M* ethylenediamine-tetraacetic acid and 0.25% trypsin. Cells were centrifuged at 500 ***g*** for 10 min.

Three cell washes with phosphate-buffered saline (PBS), centrifuging at 300 ***g*** for 10 min (220 ***g*** for 5 min for normal cells) and resuspending in 30 mL PBS, were necessary to remove the fluorescent culture medium. EEMs were measured from 3 mL suspensions in a 1 cm pathlength cuvette using a scanning Spex Fluorolog II spectrofluorimeter. Cell concentrations ranged from one to five million cells per milliliter and resulted in optically dilute samples. Samples were stirred using a magnetic stirrer to minimize cell sedimentation during data acquisition. Excitation wavelengths ranged from 250 to 550 nm in 10 nm increments, and emission wavelengths ranged from 10 nm past the excitation wavelength to the lower of 10 nm below twice the excitation wavelength or 700 nm, in 5 nm increments. Prior to and following the collection of each EEM, a cell count and trypan blue viability assay were performed. To permit background signal subtraction, a fluorescence EEM was also measured from the final supernatant for each cell line. For each cell type an EEM was measured on three different days using fresh samples. Data have been corrected for the nonuniform spectral response of the emission monochromator and detector using correction factors supplied with the instrument, and for the wavelength-dependent variations in the excitation intensity using a rhodamine B quantum counter (17). EEMs were plotted as contour maps, with contour lines connecting points of equal fluorescence intensity. Peaks were visually identified from contour maps and peak fluorescence intensities were noted at these locations.

Cellular metabolism. To assess changes in fluorescence in response to changes in metabolic state, suspensions of SiHa and HeLa cells in PBS with glucose (1000 mg/L) were perturbed by adding KCN. The concentration of glucose was chosen to match that of DMEM. After measuring the fluorescence emission spectra at 350 nm excitation, KCN was added to the cell suspension to a final concentration of 5 m*M*. Emission spectra at the same excitation wavelength were measured immediately before and after addition of KCN and at four time points from 20 to 155 min following addition. Prior to and following the experiment, a cell count and trypan blue viability assay were performed. This experiment was performed nine times (five with SiHa and four with HeLa), using different batches of cells.

RESULTS

Short-term tissue culture fluorescence

Bright-field and fluorescence images, with recognizable epithelium and stroma, were collected from 31 colposcopically normal cervical biopsies from 18 patients. The patients ranged from 19 to 58 years in age, with four patients under 30, eight patients from 30 to 39, four patients from 40 to 49 and two patients older than 50. Biopsies were obtained from 14 patients prior to LEEP and from four patients seen for colposcopy.

Eleven biopsies were imaged using the first set of filters and 20 biopsies were imaged using the second set of filters. H & E-stained sections from these biopsies were diagnosed by a board-certified pathologist as normal (six showed inflammation or a focal cluster of cells suggestive, but not diagnostic of koilocytosis).

The visual impression of the images suggested several trends in the tissue fluorescence pattern. Based on the fluorescence pattern, images from the 31 biopsies were divided into three categories: (1) slices with bright epithelial fluorescence which was generally brighter than the stromal fluorescence; (2) slices with similar fluorescence intensities in the epithelium and stroma; and (3) slices with weak epithelial fluorescence and strong stromal fluorescence.

Figure 1 shows bright-field and fluorescence images for a representative slice from each group. In cases where fluorescence was measured at 337 nm excitation, in addition to 380 and 460 nm excitation, all images are shown. The approximate size of the fluorescence and bright-field images is 1×1 mm^2. Also shown are plots of the fluorescence intensity *vs* depth throughout each slice. The intensities for different images should be comparable, however, slight variations ($\pm 10\%$) in slice thickness makes exact quantitative comparison difficult.

Fifteen image sets from 11 patients showed bright epithelial fluorescence and somewhat weaker stromal fluorescence and were placed in Group 1. In most cases, the epithelial fluorescence was not diffuse or evenly distributed. Rather, there was often a clear striped pattern, with the superficial and basal layers having brighter fluorescence than the parabasal area. From patient to patient, the thickness of the more intense stripes varied and in a few cases they were not clearly observed. The stromal fluorescence in this group was generally diffuse, but in a few cases bright spots were seen on a background of weaker fluorescence. Eleven image sets from 8 patients showed stromal fluorescence that was brighter than epithelial fluorescence and were placed in Group 2. The epithelial fluorescence in this group exhibited the same striped appearance as in Group 1 in all but one image set.

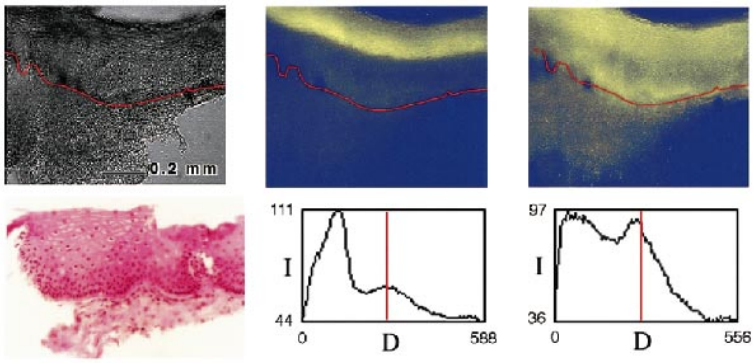

(a) Group 1 image. 20 yrs, African-American, Pathology: Normal, chronic inflammation.

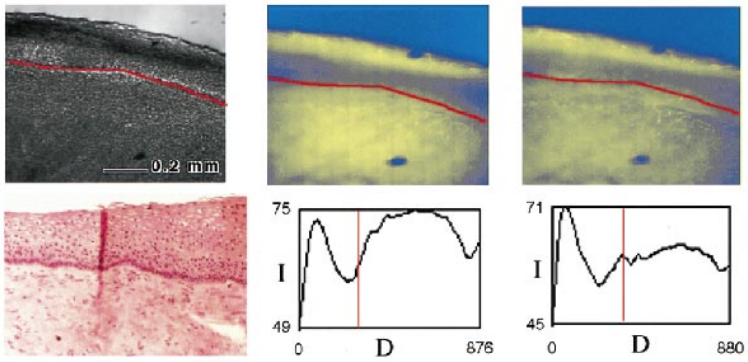

(b) Group 2 image. 40 yrs, Hispanic, Pathology: Normal.

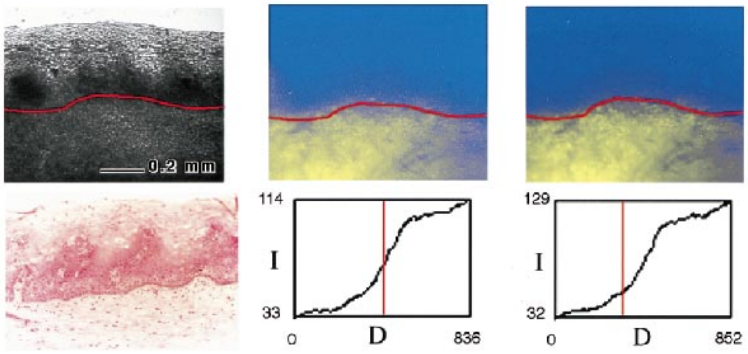

(c) Group 3 image. 49 yrs, African-American, postmenopausal. Pathology: Normal, with very focal area suggestive of koilocytosis.

Figure 1. Representative images from (a) Group 1, (b) Group 2 and (c) Group 3. Each image set includes the bright-field and fluorescence images, the corresponding H & E image and plots of fluorescence intensity *vs* depth for each excitation wavelength. Vertical red lines on the intensity plots indicate the approximate location of the basement membrane. The sample shown from Group 1 was obtained from a 20 year–old African American woman; histology showed chronic inflammation. The sample shown from Group 2 was obtained from a 40 year–old Hispanic woman; histology showed no evidence of disease. The sample shown from Group 3 was obtained from a 49 year–old African American woman; histology showed a very focal area suggestive, but not diagnostic of koilocytosis.

In some cases the bright stromal fluorescence was associated with distinct bright spots, and in other cases the entire stroma was quite bright. Five image sets from 5 women showed stromal fluorescence that was much more intense than that in the epithelium and were placed in Group 3. These images appeared quite different from those in the previous two groups, due to the weaker epithelial fluorescence.

A strong correlation was observed between age and the fluorescence pattern (Fig. 2). The average age of Group 1 patients is 30.9 years, and only one of the 11 patients is postmenopausal. The average age of the women in Group 2 is 38.0, and three of the eight patients were postmenopausal. In Group 3, the average age is 49.2 years and four of the five women are postmenopausal. Differences in the average age of patients in each of the groups were statistically significant at or below the $P = 0.05$ level using a one-tailed Student's *t*-test.

The average fluorescence intensity (in arbitrary units) of the epithelium and stroma was calculated for each group, obtained using the second set of filters at 380 and 460 nm

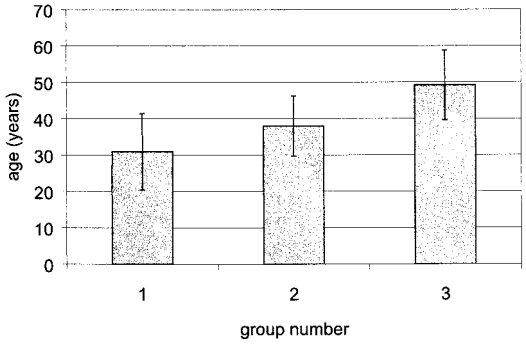

Figure 2. Average age of patients represented in Groups 1, 2 and 3. Error bars represent two standard deviations.

excitation (Fig. 3). In Group 1, the average epithelial fluorescence was greater than the average stromal fluorescence. In Group 2 average epithelial and stromal fluorescence intensities were comparable. In Groups 2 and 3, the average stromal fluorescence was more intense than the average epithelial fluorescence. The average intensity of the epithelial fluorescence was similar in Groups 1 and 2, but was lower in Group 3; these differences were not statistically significant at or below the $P = 0.10$ level at 380 and 460 nm excitation. However, the average stromal fluorescence was similar in Groups 2 and 3, and lower in Group 1; these differences were significant below the $P = 0.05$ level at 380 and 460 nm excitation using a one-tailed Student's *t*-test.

In addition, for each image, the ratio of mean epithelial fluorescence to mean stromal fluorescence was calculated for all 31 samples (Fig. 4). The average ratio was then computed and compared for each group. The average ratios were found to be 1.20, 0.87 and 0.61 at 380 nm excitation, and 1.22, 0.87 and 0.63 at 460 nm excitation, for Groups 1, 2 and 3, respectively. The ratios were statistically different for each of the three groups using a one-tailed Student's *t*-test. ($P < 0.01$).

To determine the presence and distribution of collagen and elastin, two histological staining protocols were used. No staining for elastin occurred, but abundant collagen was observed in the stroma.

EEMs of cell suspensions

EEMs of HeLa, SiHa, TCL-1 and normal cervical cell types showed four major peaks, which were consistent with the

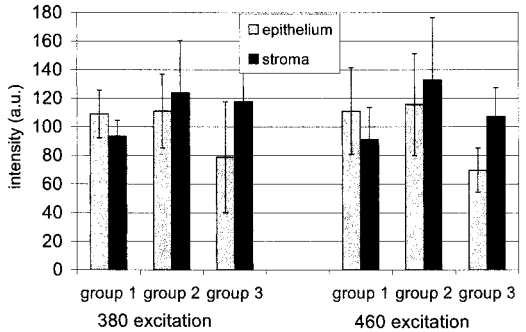

Figure 3. Average intensity in the epithelium and stroma for samples in Groups 1, 2 and 3 at 380 nm and 460 nm excitation. Error bars represent two standard deviations.

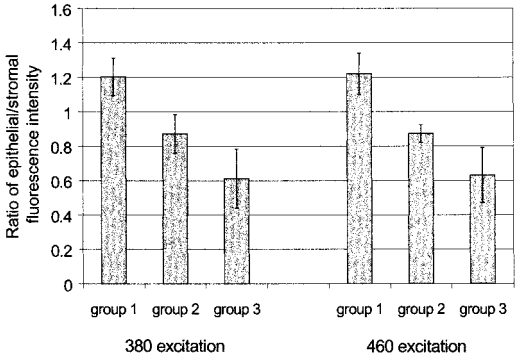

Figure 4. Comparison of the ratio of fluorescence intensity in the epithelium and stroma for each group at 380 and 460 nm excitation. Error bars represent two standard deviations.

fluorophores tryptophan, NADH and FAD. In all cases, the most intense peak was seen at 290 nm excitation, 330 nm emission, corresponding to tryptophan. Additional peaks were located at 370 nm excitation, 440 nm emission, corresponding to NADH and FAD and at 370 and 450 nm excitation, 530 nm emission, also corresponding to FAD. The tryptophan fluorescence was two orders of magnitude higher than that of NADH, which was four to seven times more intense than that of FAD. An EEM measured from the SiHa cells is shown in Fig. 5.

Response of cell suspension fluorescence to KCN

Fluorescence intensities at 350 nm excitation were measured for suspensions of SiHa and HeLa cells in PBS with glucose before the addition of KCN, and at intervals during a 1–2 h incubation with KCN. The peak fluorescence intensity increased by 29–37% in five runs of this experiment with SiHa cells, with peak fluorescence noted at 20–60 min following addition of KCN. The fluorescence intensity increased by 39–50% in three of four runs of the experiment with HeLa cells, reaching a maximum 0–30 min after addition of KCN. In one run of the experiment, no change in fluorescence intensity was observed. These results are consistent with an increased concentration of NADH following the addition of

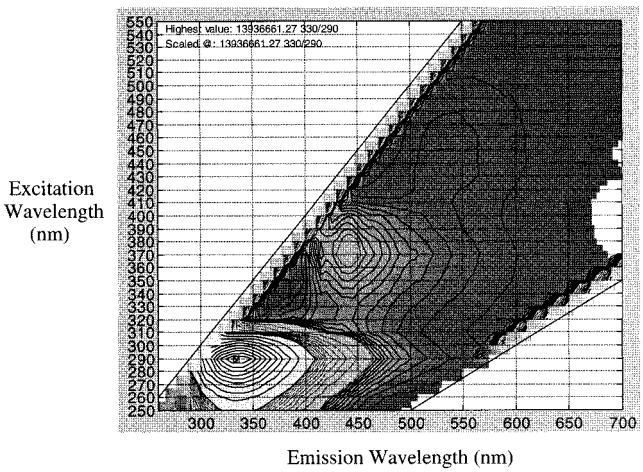

Figure 5. Fluorescence EEMs of a suspension of SiHa cells.

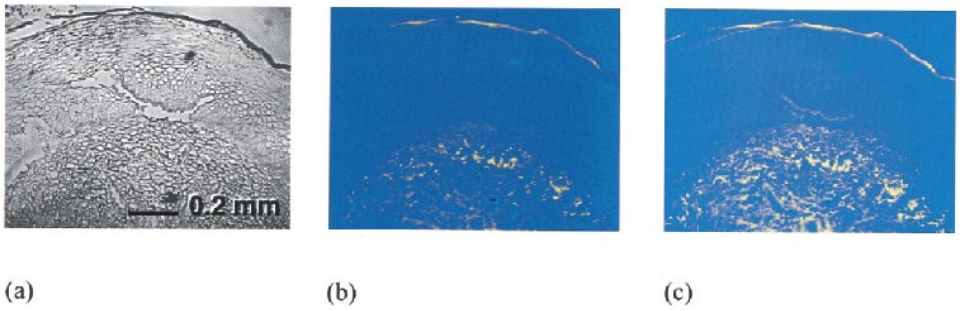

Figure 6. (a) Bright-field and fluorescence images at (b) 380 nm and (c) 460 nm excitation of frozen–thawed cryosections obtained from a normal cervical biopsy.

KCN and support the hypothesis that the signal measured at 350 nm excitation reflects the NADH level.

Response of slice fluorescence to KCN

KCN was also used to perturb the metabolic state of several short-term tissue cultures and determine if any changes in fluorescence occurred in response. In two runs of this experiment, the epithelial fluorescence increased by 25% with the addition of KCN, and then decreased by 15% when the slice was returned to medium without KCN. These results are consistent with the expected effect of KCN, and an increased concentration of NADH.

DISCUSSION

In this study, autofluorescence patterns of normal cervical tissue were characterized using short-term tissue cultures. Short-term tissue cultures can be made thin enough to resolve tissue structure and can be maintained in culture medium for up to 24 h without special precautions. Therefore, they represent a novel model system for mapping cervical tissue fluorescence to particular tissue layers and chromophores.

The fluorescence patterns observed from short-term tissue cultures are in contrast to those previously reported in frozen–thawed cervical tissues (7,8). Images of cervical frozen–thawed cryosections show very weak epithelial fluorescence, except in the most superficial layer, and brighter stromal fluorescence. Representative bright-field and fluorescence images from 4 μm–thick cervical cryosections, obtained in this laboratory, are shown in Fig. 6. Very little epithelial fluorescence is observed in any sections; the lack of epithelial fluorescence is consistent from one patient to another. The differences in fluorescence imaged from fresh and frozen tissues suggest that models of tissue fluorescence, such as that developed by Zonios *et al.*, need different inputs to accurately describe the *in vivo* situation.

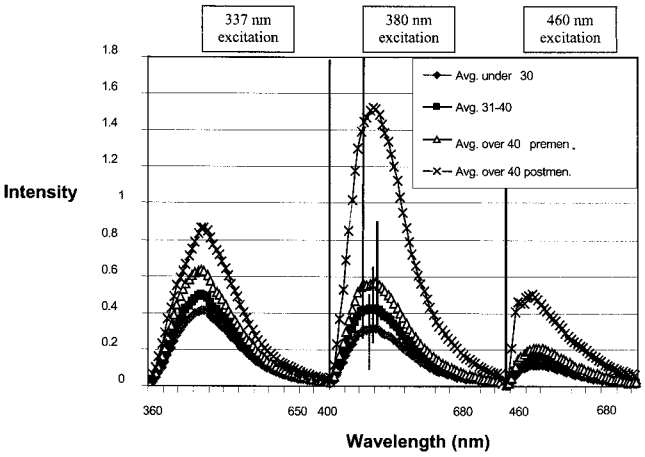

Figure 7. Average flourescence spectra at 337, 380 and 460 nm excitation from squamous normal sites in the intact cervix vs. patient age. Data are shown from 106 sites in 51 patients; 16 sites were from patients under 30 years of age, 55 sites were from patients 31–40, 21 sites were from premenopausal patients over 40 and 14 sites were from postmenopausal patients over 40 years of age.

The fluorescence patterns observed in this study suggest three patterns of autofluorescence. The average age of the patients in each group showed a dramatic correlation between fluorescence pattern and patient age, with epithelial fluorescence decreasing with age and stromal fluorescence increasing with age. Histologic staining suggests that the stromal fluorescence may be associated with collagen. It should be noted that the fluorescence of the collagen matrix in short-term tissue cultures may differ from the *in vivo* signal, because of the tension under which it always exists *in vivo.* Nevertheless, an increase in collagen fluorescence with age is biologically plausible, because collagen fluorescence is attributed to its crosslinks (18,19), and the amount of crosslinking increases with age (20). At the same time, postmenopausal older women may experience atrophy of the cervical epithelium; in this study, the average epithelial thickness decreased from 454 ± 156 μm in Group 1, to 379 ± 148 μm in Group 2 to 305 ± 53 μm in Group 3.

These results suggest a biological basis for the increased fluorescence intensity that is seen when fluorescence is measured *in vivo* from the intact cervix in older and postmenopausal women (Fig. 7) (3). This figure shows an increase in the fluorescence intensity of squamous normal sites at 337, 380 and 460 nm excitation with age. During *in vivo* measurements, excitation light is incident upon the epithelium, and must travel through this tissue layer before reaching the stroma. The thinner, atrophic epithelium in older women may provide an easier path to the stroma for excitation light to reach the more highly crosslinked collagen.

Fluorescence measurements of cervical epithelial cell fluorescence indicate fluorescence peaks were consistent with tryptophan, NADH and FAD. Metabolic perturbation of both cell suspensions and short-term tissue cultures with

KCN resulted in increased fluorescence at UV excitation, supporting the idea that epithelial fluorescence at this wavelength is related to the NADH concentration in the cells. In the tissue slices, the increased fluorescence intensity was seen in the basal and superficial layers of the epithelium, suggesting that NADH is important in both of these regions. Additional experiments will be necessary to definitively identify the fluorophore, or fluorophores, in the superficial epithelium. However, the variations in epithelial fluorescence patterns, even within the three groups defined here, suggest that more than one type of fluorophore may be involved. It is not clear why epithelial fluorescence would be modulated with age, but there is decreased estrogen, decreased cell turnover and metabolic activity with age, all of which may affect epithelial cell fluorescence.

While a larger sample size and perhaps additional histological stains are needed to definitively assign tissue fluorophores to the fluorescence seen here in tissue slices, our results demonstrate the application of short-term tissue cultures to the investigation of cervical autofluorescence patterns. This experimental system will be important for future investigations of the spectral differences observed between normal and dysplastic tissues, and can easily be applied to additional tissue types, such as head and neck cancers.

Acknowledgements—We acknowledge the contributions of Dafna Lotan, Kathy Nolan, Judy Sandella, Alma Sbach and John Wright in the collection and preparation of specimens. Financial support from the National Cancer Institute (CA72650) and from the National Institute of Dental and Craniofacial Research (P50 DE11906) are gratefully acknowledged.

REFERENCES

1. Ramanujam, N., M. F. Mitchell, A. Mahadevan, S. Thomsen, A. Malpica, T. Wright, N. Atkinson and R. Richards-Kortum (1996) Development of a multivariate statistical algorithm to analyze human cervical tissue fluorescence spectra acquired in vivo. *Lasers Surg. Med.* **19**, 46–62.
2. Ramanujam, N., M. F. Mitchell, A. Mahadevan, S. Thomsen, A. Malpica, T. Wright, N. Atkinson and R. Richards-Kortum (1996) Spectroscopic diagnosis of cervical intraepithelial neoplasia (CIN) in vivo using laser-induced fluorescence spectra at multiple excitation wavelengths. *Lasers Surg. Med.* **19**, 63–74.
3. Ramanujam, N., M. F. Mitchell, A. Mahadevan-Jansen, S. Thomsen, A. Malpica, T. Wright, N. Atkinson and R. Richards-Kortum (1996) Cervical precancer detection using a multivariate statistical algorithm based on laser-induced fluorescence spectra at multiple excitation wavelengths. *Photochem. Photobiol.* **64**, 720–735.
4. Glassman, W. S., C. H. Liu, G. C. Tang, S. Lubicz and R. R. Alfano (1992) Excitation spectroscopy of malignant and non-malignant gynecological tissues. *Lasers Life Sci.* **5**, 49–58.
5. Lohmann, W., J. Mußmann, C. Lohmann and W. Kunzel (1989) Native fluorescence of the cervix uteri as a marker for dysplasia and invasive carcinoma. *Eur. J. Obstet. Gynecol. Reprod. Biol.* **31**, 249–253.
6. Ramanujam, N., M. F. Mitchell, A. Mahadevan, S. Thomsen, A. Malpica, T. Wright, N. Atkinson and R. Richards-Kortum (1994) In vivo diagnosis of cervical intraepithelial neoplasia using 337-nm-excited laser-induced fluorescence. *Proc. Natl. Acad. Sci. USA* **91**, 10 193–10 197.
7. Lohmann, W., J. Mussman, C. Lohmann and W. Kunzel (1989) Native fluorescence of unstained cryo-sections of the cervix uteri compared with histological observation. *Naturwissenschaften* **96**, 125–127.
8. Mahadevan, A. (1998) Fluorescence and Raman spectroscopy for diagnosis of cervical precancers. Thesis, The University of Texas at Austin, Austin, TX.
9. Durkin, A. J. and R. R. Richards-Kortum (1996) Comparison of methods to determine chromophore concentrations from fluorescence spectra of turbid samples. *Lasers Surg. Med.* **19**, 75–89.
10. Zonios, G., R. Cothren, J. Arendt, J. Wu, J. Van Dam, J. Crawford, R. Manoharan and M. S. Feld (1996) Morphological model of human colon tissue fluorescence. *IEEE Trans. BME* **43**, 113–122.
11. Schomacker, K. T., J. K. Frisoli, C. C. Compton, T. J. Flotte, J. M. Richter, N. S. Nishioka and T. F. Deutsch (1992) Ultraviolet laser-induced fluorescence of colonic tissue: basic biology and diagnostic potential. *Lasers Surg. Med.* **12**, 63–78.
12. Krumdieck, C. L., J. Ernesto Dos Santos and K. Ho (1980) A new instrument for the rapid preparation of tissue slices. *Anal. Biochem.* **104**, 118–123.
13. Smith, P. F., A. J. Gandolfi, C. L. Krumdieck, C. W. Putnam, C. F. Zukoski, W. M. Davis and K. Brendel (1985) Dynamic organ culture of precision liver slices for in vitro toxicology. *Life Sci.* **36**, 1367–1375.
14. Smith, P. F., G. Krack, R. L. McKee, D. G. Johnson, A. J. Gandolfi, V. J. Hruby, C. L. Krumdieck and K. Brendel (1986) Maintenance of adult rat liver slices in dynamic organ culture. *In Vitro Cell. Dev. Biol.* **22**, 706–712.
15. Sahlin, K. and A. Katz (1986) The content of NADH in rat skeletal muscle at rest and after cyanide poisoning. *Biochem. J.* **239**, 245–248.
16. Carson, F. L. (1990) *Histotechnology: A Self-Instructional Text*. ASCP Press, Chicago.
17. Taylor, D. G. and J. N. Demas (1979) Light intensity measurements. I. Large area bolometers with microwatt sensitivities and absolute calibration of the Rhodamine B quantum counter. *Anal. Chem.* **51**, 712–717.
18. Fujimoto, D. (1977) Isolation and characterization of a fluorescent material in bovine achilles tendon collagen. *Biochem. Biophys. Res. Commun.* **76** 1124–1129.
19. Eyre, D. and M. Poz (1984) Cross-linking in collagen and elastin. *Annu. Rev. Biochem.* **53**, 717–748.
20. Bailey, A. J., R. G. Paul and L. Knott (1998) Mechanisms of maturation and ageing of collagen. *Mech. Ageing Dev.* **106**, 1–56.